



Evaluation of Partially Averaged Navier-Stokes Method in Simulating Flow Past a Sphere

S. Saroha^{1†}, S. S. Sinha¹, and S. Lakshmipathy²

¹ Applied Mechanics Department, IIT Delhi, 110016, India

² Gexcon AS, Bergen, 5072, Norway

[†] Corresponding Author Email: sagarsaroha18@gmail.com

(Received January 4, 2018; accepted April 15, 2018)

ABSTRACT

In recent past partially averaged Navier-Stokes equation (PANS) has been proposed as a scale-resolving bridging method for turbulence computations. Despite the geometric simplicity of the involved boundary conditions, the flow past a sphere is ripe with various complex flow phenomena, which make it an excellent test bed to evaluate various computational fluid dynamics modelling methodologies – both in terms of numerical schemes as well as turbulence models. Specifically, in this work we evaluate PANS in conjugation with the standard $k-\epsilon$ model in terms of (i) influence of filter parameters, (ii) sensitivity to free stream viscosity ratio and (iii) choice of numerical schemes at supercritical Reynolds number of 1.14×10^6 . Careful evaluations are made by comparing PANS results against available experimental data as well available detached eddy simulation (DES) and large eddy simulation (LES) results. Our study finds that indeed – as purported by the PANS theory – a reduction in the value of the first filter parameter (f_k) successfully captures the complex vortical structures that exist past a sphere, shows far superior performance than unsteady Reynolds-averaged Navier-Stokes (URANS) simulations and somewhat improved performance even over some of the LES studies reported in literature. Our study shows that in terms of most of the quantities of interest, PANS performance is almost at par with that of DES.

Keywords: Computational Study; Scale-resolving methods; High Reynolds number; Flow past a sphere.

NOMENCLATURE

C_D	drag coefficient	ρ	density of fluid
C_p	pressure coefficient	V_∞	freestream velocity of fluid
C_f	skin friction coefficient	V	velocity of fluid
F_x	force on sphere along streamwise direction	A	projected area of sphere
τ_w	wall shear stress	D	sphere diameter
Ω_{ij}	rotation-rate tensor	P	pressure
S_{mn}	strain-rate tensor	p_∞	freestream pressure

1. INTRODUCTION

Despite the simple geometry of a sphere, flow past it at high Reynolds number (Re) is quite complex, involving the concurrence of several complicated flow phenomena: large-scale unsteadiness and Reynolds number-dependent three-dimensional vortex shedding patterns multiple instability modes, laminar to turbulent

transition and massive separation [Achenbach (1974), Drikakis (1995), Jindal *et al.* (2004)]. Co-existence of these multiple flow phenomena has not only motivated many experimental studies [Achenbach (1972), Achenbach (1974), Taneda (1978)], it has also made the flow past a sphere a unique and one of the most demanding benchmark cases for testing computational fluid dynamic methods - in terms of both the discretization schemes as well as turbulence models [Constantinescu and Squires (2000),

Constantinescu and Squires (2004)]. The focus of this work is to evaluate the so-called partially averaged Navier-Stokes (PANS) method of turbulence in simulating flow past a sphere at adequately high Reynolds number (1.14×10^6) when all the aforementioned flow features are known to exist.

Application of direct numerical simulation (DNS) for flow past a sphere has been restricted to sub-critical Reynolds number only. Shirayama and Kuwahara (1992), Gebing (1992), Aliabadi and Tezduyar (1995), Shen and Loc (1997), Kalro and Tezduyar (1998), Mansoorzadeh *et al.* (1998) and Johnson and Patel (1999) have performed DNS studies with Reynolds number up to 10^3 . Seidl *et al.* (1997) performed DNS studies at $Re = 5000$; Kim and Choi (2001) and Bazilevs *et al.* (2014) has performed their study at $Re = 10^4$.

Despite its reasonable acceptability in several other flows of practical interest, Reynolds-averaged Navier-Stokes (RANS) and even its unsteady counterpart - Unsteady RANS (URANS) have been found to be severely inadequate for simulating flow past a sphere. Drikakis (1995) performed simulation of flow past a sphere at $Re_D = 10^5$ and 10^6 using URANS in conjunction with the $k-\epsilon$ model. While the pressure distribution upstream of the separation point was found to be adequate, the same in the post-separation regime shows large errors. Further, the URANS method could not capture any unsteadiness at all. Based on their studies, Tomboulides and Orszag (2000) concluded that due to the reduced coherence of shed structures in flow past a sphere (as compared to a cylinder), the resolution of finer flow features are essential to correctly capture the vortex shedding and three dimensionality which dominate the flow behaviour past a sphere. Since it indiscriminately suppresses all fine scale unsteadiness, irrespective of the choice of turbulence model, URANS has been judged to be inherently unsuitable for simulating various features of the flow past a sphere (Constantinescu and Squires 2003b).

In recent years, researchers have attempted to address the gap between DNS and URANS by using scale-resolving methods or filter-based methods for simulating the flow past a sphere. Two such methods – large eddy simulation (LES) and detached eddy simulation (DES) – have been employed by several workers to simulate the flow past a sphere at high Reynolds numbers. LES uses a filter cutoff: all scales below that cutoff scale are modelled, whereas scales larger than that are solved directly (resolved). The cutoff length scale in LES is typically chosen near the dissipation range of the spectrum so that the burden and the uncertainty incurred while modeling the unresolved motion is meagre. This allows for the application of simple

Samargorinsky-like algebraic (zero-equation) closures. However, given that the cutoff length scale in LES is close to the typical dissipation range, the reduction in computational burden in LES as compared to DNS is limited. A part of this problem is addressed by the so-called detached eddy simulation method wherein the formulation behaves like LES in the bulk of the flow and switches to RANS in the near-wall zones. DES uses the Spalart-Allmaras (SA) model in the near-wall region in conjunction with the RANS equations. By switching to RANS variables in the near-wall region DES avoids the burden of resolving small scale motion in the near-wall region (thus reducing the burden of having a very fine mesh there) and at the same time, uses the capability of LES to reliably resolve wider scales of motion in regions away from walls. Tomboulides *et al.* (1993) have performed LES simulations of flow past a sphere at $Re_D = 2 \times 10^4$. They used a subgrid model based on the renormalization group theory. Several other LES-based studies have been performed by Kim and Durbin (1988), Kim and Choi (2001), Schmidt (2002), Jindal *et al.* (2004), Constantinescu and Squires (2003a). Constantinescu and Squires (2003b) have employed and validated the DES method in flow past the sphere over a range of Reynolds number (10^4 - 10^6). Based on our literature review, we deem the DES results of Constantinescu and Squires (2004) to be the state-of-the-art numerical results for the flow past a sphere at Reynolds number of 1.14×10^6 .

Partially averaged Navier-Stokes (PANS) method has emerged as a new promising paradigm of turbulence computation. While PANS, like LES and DES, is a filter-based or a scale-resolving method, it is purported to be more versatile than both LES and DES. Girimaji (2006) proposed PANS as a *bridging method* which uses two implicit filtering parameters: f_k and f_ϵ . The parameter f_k is ratio of the unresolved kinetic energy in PANS to the un-resolved kinetic energy in a corresponding URANS simulation, whereas f_ϵ is the ratio of unresolved dissipation-rate in PANS to that in URANS simulation (more details in Section 2). Unlike the LES or DES in which the filter cutoff is typically placed near the dissipation range, PANS allows the user to change the filter parameter seamlessly, encompassing large to inertial to dissipative range of motion. Setting $f_k = 1$ and $f_\epsilon = 1$ makes PANS equivalent to RANS, whereas $f_k = 0$ and $f_\epsilon = 1$ makes PANS equivalent to DNS. With this flexibility, depending on the size of the grid that the user can afford to have, the filtering parameter can be chosen anywhere between the two extremes of RANS and DNS. Further, it is argued that unlike DES and other hybrid RANS/LES methods, PANS is a superior scale-

resolving method because its formulation is completely consistent with the averaging invariance property of the Navier-Stokes equation [Germano (1992), Girimaji (2006), Suman and Girimaji (2010)].

In recent years, PANS method has been evaluated in a variety of both canonical and practical flows of interest and the performance has been found to be quite encouraging. To further evaluate the performance of PANS method, in this work we subject PANS to its (perhaps) the most severe test: massively separated three-dimensional flow past a sphere at high Reynolds number. The authors believe that such an evaluation is essential to extensively benchmark the PANS method in extremely challenging flow environment (co-existence of large scale unsteadiness, massive three-dimensional flow separation, presence of several instability modes) and identify its shortcomings, if any. Naturally, it is expected that this critical examination may lead to further improvements of PANS. With this motivation, we examine the performance of PANS model in flow past a sphere specifically in terms of:

- i. Influence of discretization schemes;
- ii. Influence of varying f_k and examining if indeed PANS formulation captures increasing unsteadiness and finer scales of motion when f_k is decreased (as theoretically purported);
- iii. Influence of free stream turbulence;
- iv. Influence of the second filtering parameter, f_e on PANS performance.

In this study all our computations are performed at $Re = 1.14 \times 10^6$ and comparisons are made against available experimental (Achenbach 1974), LES (Kim and Choi 2001) and DES (Constantinescu and Squires 2004) results. Extensive comparisons are made in terms of various near-wall and wake-related statistical quantities. Further, flow structures are examined using instantaneous flow fields.

This paper is organized into six sections. In section 2 we provide a brief review of PANS methodology and list the governing equations. In section 3 we present details of our computational set-up. In section 4 we present the plan of our study. In section 5 we present our results and pertinent discussion. Section 6 concludes the paper with a summary.

2. PARTIALLY AVERAGED NAVIER-STOKES

In this section, we provide a brief overview of PANS methodology and its purported superiority over URANS method. For full details of the PANS methodology, the reader is referred to

Girimaji (2006).

We begin with the instantaneous Navier-Stokes equations for an incompressible flow:

$$\frac{\partial V_i}{\partial t} + V_j \frac{\partial V_i}{\partial x_j} = -\frac{1}{\rho} \frac{\partial p}{\partial x_i} + \nu \frac{\partial^2 V_i}{\partial x_j \partial x_j}; \quad (1)$$

$$\frac{1}{\rho} \frac{\partial^2 p}{\partial x_i \partial x_i} = -\frac{\partial V_i}{\partial x_j} \frac{\partial V_j}{\partial x_i}; \quad (2)$$

where V_i , p and ρ represent instantaneous velocity, pressure and density. The symbol ν is kinematic viscosity and the symbol t & x_i represent time & spatial coordinates. Equation 2 is the Poisson's equation of pressure. This equation is obtained by subjecting the momentum equation to the divergence operator, and subsequently using the continuity equation for incompressible flow, $\frac{\partial V_i}{\partial x_i} = 0$.

PANS equations are obtained by applying a partial-averaging filter to the instantaneous incompressible flow equations. Correspondingly the filtered fields are $\langle V_i \rangle$ ($\equiv U_i$) and $\langle p \rangle$ ($\equiv p_u$), where $\langle \rangle$ represents the partial-averaging filter. Assuming that the filter is constant preserving, and that it commutes with spatial and temporal derivative operators (Girimaji 2006), the governing equations of U_i and p_u obtained are:

$$\frac{\partial U_i}{\partial t} + U_j \frac{\partial U_i}{\partial x_j} + \frac{\partial \tau(V_i, V_j)}{\partial x_j} = \quad (3)$$

$$-\frac{1}{\rho} \frac{\partial p_u}{\partial x_i} + \nu \frac{\partial^2 U_i}{\partial x_j \partial x_j};$$

$$\frac{1}{\rho} \frac{\partial^2 p_u}{\partial x_i \partial x_i} = -\frac{\partial U_i}{\partial x_j} \frac{\partial U_j}{\partial x_i} - \frac{\partial^2 \tau(V_i, V_j)}{\partial x_i \partial x_j}. \quad (4)$$

The quantity $\tau(V_i, V_j)$ is called the generalized central moment of V_i and V_j in accordance with the definition of Germano (1992):

$$\tau(V_i, V_j) = \langle V_i V_j \rangle - \langle V_i \rangle \langle V_j \rangle. \quad (5)$$

In Eqs. (3) and (4), $\tau(V_i, V_j)$ is the unclosed quantity. In this work, we employ the PANS version of Boussinesq eddy viscosity assumption (Girimaji 2006) to tackle this:

$$\tau(V_i, V_j) = \frac{2}{3} k_u \delta_{ij} - 2\nu_u S_{ij}; \quad (6)$$

where ν_u is unresolved eddy viscosity and S_{ij} is

$$\text{the filtered strain-rate: } S_{ij} = \frac{1}{2} \left(\frac{\partial U_i}{\partial x_j} + \frac{\partial U_j}{\partial x_i} \right).$$

The unresolved eddy viscosity (ν_u) is related to unresolved kinetic energy (k_u) and unresolved

dissipation-rate (ε_u) as: $v_u = C_\mu \frac{k_u^2}{\varepsilon_u}$, where C_μ is a model coefficient. These quantities k_u and ε_u can be expressed as generalised central moments:

$$k_u = \frac{1}{2} \tau(V_i, V_i); \quad \varepsilon_u = \nu \tau \left(\frac{\partial V_i}{\partial x_j}, \frac{\partial V_i}{\partial x_j} \right).$$

Finally, the closure is achieved by including the evolution equations of k_u and ε_u . Using f_k and f_ε (the filter control parameters of PANS), the modeled evolution equation of k_u and ε_u are:

$$\frac{\partial k_u}{\partial t} + U_j \frac{\partial k_u}{\partial x_j} = P_u - \varepsilon_u + \frac{\partial}{\partial x_j} \left(\left(\frac{v_u}{\sigma_{k_u}} + \nu \right) \frac{\partial k_u}{\partial x_j} \right); \quad (7)$$

$$\begin{aligned} \frac{\partial \varepsilon_u}{\partial t} + U_j \frac{\partial \varepsilon_u}{\partial x_j} = & f_k \left(C_{\varepsilon 1} \frac{P_u \varepsilon_u}{k_u} - C_{\varepsilon 2}^* \frac{\varepsilon_u^2}{k_u} \right) \\ & + \frac{\partial}{\partial x_j} \left(\left(\frac{v_u}{\sigma_{\varepsilon_u}} + \nu \right) \frac{\partial \varepsilon_u}{\partial x_j} \right); \end{aligned} \quad (8)$$

where, $f_k = k_u/k$ and $f_\varepsilon = \varepsilon_u/\varepsilon$; k and ε are turbulence kinetic energy and its dissipation rate. The quantity P_u is production of unresolved kinetic energy: $P_u = \tau(V_i, V_j) \frac{\partial U_i}{\partial X_j}$; the symbols

σ_{k_u} and σ_{ε_u} are turbulent prandtl numbers for unresolved kinetic energy and dissipation rate.

The modified model coefficients appearing in Eqs. (7) and (8) are (Girimaji and Abdol-Hamid 2005):

$$C_{\varepsilon 2}^* = C_{\varepsilon 1} + \frac{f_k}{f_\varepsilon} (C_{\varepsilon 2} - C_{\varepsilon 1}); \quad (9)$$

$$\sigma_{k_u} = \sigma_k \frac{f_k^2}{f_\varepsilon}; \quad \sigma_{\varepsilon_u} = \sigma_\varepsilon \frac{f_k^2}{f_\varepsilon}. \quad (10)$$

Other model coefficients hold the same values as in standard $k-\varepsilon$ model. $C_{\varepsilon 1} = 1.44, C_{\varepsilon 2} = 1.92, \sigma_{k_u} = 1.0, \sigma_{\varepsilon_u} = 1.3$. Equations (3), (4), (6), (7) and (8) form a closed set of PANS equations employing standard $k-\varepsilon$ model and the Boussinesq eddy-viscosity approximation.

The value of v_u can be controlled by choosing apt values of filter-width control parameters. Choosing a sub-unity value of f_k reduces the production of turbulent kinetic energy, which in turn can reduce v_u , allowing for more scales to be released and resolved. On the other hand, reducing the value of f_ε can reduce the dissipation-rate of turbulence kinetic energy, which in turn has the opposite effect of leading to larger accumulation of kinetic energy in the flow domain and consequently suppressing unsteadiness in the flow field. These two control

parameters can be used to adjust the overall level of v_u so that a PANS simulation can generate and resolve a range of scales which is commensurate with the fineness of the grid specified by the user.

3. COMPUTATIONAL SET-UP

The computational domain employed in this study is a cylindrical volume with diameter being 10 times and the length being 15 times the sphere diameter (D). The centre of the sphere is located at $5D$ from the upstream boundary. A schematic of the domain is shown in Fig. 1.

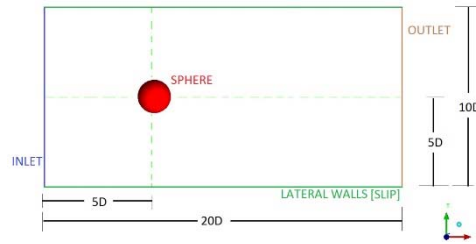


Fig. 1. Schematic of Computational Domain

For our simulations we employ an unstructured mesh consisting of prism layers and tetra elements similar to that used by Bazilevs *et al.* (2014). The height of the prism layer is chosen such that the boundary layer is resolved within prism elements. The y^+ value of the first node in near wall region is ensured to be sub-unity. Density boxes are used to control element sizing around the sphere and in the wake region. The total mesh element count is 1.8 million. The count of prism cells is 0.5 million and the rest are tetra elements. Figure 2 shows screenshots of the mesh.

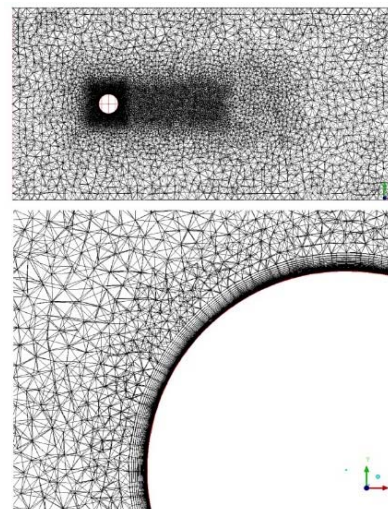


Fig. 2. 2D slice ($Z=0$ plane) of the mesh used for computations

The solver used in this study is ANSYS FLUENT, which is industry-standard for internal/external fluid flows and flows involving heat transfer. FLUENT facilitates appropriate

modification of turbulence model coefficients in a relatively simpler way, thus enabling implementation of PANS methodology [Eqs. (3), (4), (6), (7) and (8)].

For near-wall treatment, we employ the two-layer approach developed by [Chen and Patel \(1988\)](#). The near-surface region is divided into a viscosity-affected layer and a fully-turbulent region. Demarcation of the two regions and the length scale in the inner layer is determined using turbulent Reynolds number. In the viscosity affected inner layer, one equation model is solved – retaining the momentum and kinetic energy Eq. (7). In fully turbulent/outer region, complete two-equation model is employed with active dissipation rate Eq. (8). Since instead of using the wall function approximations, one equation model is solved in inner layer, the value of first near-wall node is ensured to be near unity. ([Chen and Patel 1988](#))

In this study, results from several simulations are presented. In all these simulations, no-slip boundary and no-penetration conditions are specified at the sphere surface and the free-slip boundary condition is specified at lateral walls with zero shear stress. At the exit/outlet of the computational domain outflow boundary condition is used. Inlet boundary conditions are specified in terms of the velocity and turbulence variables. The free stream turbulence condition at the inlet of the domain is parameterized in terms of the viscosity ratio (η_r) using following relations [[Constantinescu and Squires \(2003b\)](#), [Han *et al.* \(2012\)](#)]:

$$\eta_r = \frac{v_u}{v} = \frac{C_\mu k_u^2}{\varepsilon_u} \frac{1}{v}; k_u = \frac{3}{2}(V_\infty I)^2; \quad (11)$$

$$\varepsilon_u = \frac{C_\mu k_u^2}{v} \frac{1}{\eta_r}$$

Table 3 Computational Settings

Solver	Pressure-based
Type	3D Transient Implicit
Turbulence Model	Standard $k - \varepsilon$ model
Wall treatment	Two layer treatment
Pressure-Velocity coupling	SIMPLE
Gradient	Least Square Cell Based
Pressure	Second Order
Momentum, TKE, TDR	BCD/ SOU/ MUSCL
Transient	Bounded 2 nd -Order Implicit

where V_∞ is free stream velocity, I is turbulent intensity, C_μ is model coefficient from standard $k - \varepsilon$ model (0.09), v is laminar viscosity and v_u is

unresolved turbulent viscosity. Interior of the domain is initialized with the value of turbulence kinetic energy and dissipation rate picked from the inlet.

In Table 3, we present a summary of the solver settings employed in all our simulations. We have used a pressure-based solver. Pressure-velocity coupling is addressed employing the SIMPLE algorithm. For convective terms in the momentum equation one of the following schemes – third order MUSCL, bounded central difference (BCD) or second order upwind (SOU) – is employed. Other gradient terms are discretized using the least square cell based method. For temporal discretization bounded second order fully implicit method is used.

We perform our simulations at $Re = 1.14 \times 10^6$, which is in the supercritical regime of flow past a sphere. In supercritical regime the flow is already turbulent in boundary layer before separation happens. Since the two-layer $k - \varepsilon$ model estimates length scale in near-wall region using turbulent Reynolds number, it is inappropriate for prediction of flow involving laminar separation. Thus, we assume the boundary layer to be turbulent throughout. Simulations with this assumption have been performed by other workers as well [[Constantinescu and Squires \(2003b\)](#), [Jones and Clarke \(2008\)](#)]. For sensible comparisons, we employ relevant experimental data with fully turbulent boundary layer, which is available at Reynolds number of 1.14×10^6 ([Achenbach 1974](#)).

Table 4 Simulation Cases

Case	Scheme	f_k	f_ε	v_u/v	CFL
X01	MUSCL	0.5	1.0	10	4
X02	MUSCL	0.5	1.0	10	2
X03	MUSCL	0.5	1.0	10	1
X04	SOU	0.5	1.0	10	1
X05	BCD	0.5	1.0	10	1
X06	MUSCL	0.5	1.0	1	1
X07	MUSCL	0.5	1.0	100	1
X08	MUSCL	0.7	1.0	10	1
X09	MUSCL	1.0	1.0	10	1
X10	MUSCL	0.5	0.5	10	1
X11	MUSCL	0.7	0.7	10	1

4. PLAN OF STUDY & QUANTITIES OF INTEREST

For this study, in total 11 different simulations (X01-X11) have been performed. Table 4

presents an overview of the variations in the simulation settings. All these simulations have been performed on the same grid which is described in Section 3.

As outlined in the introduction (Section 1), we intend to comprehensively evaluate the performance of PANS method in simulating the flow past a sphere in terms of (i) Choice of discretization scheme, (ii) Influence of f_k , (iii) Influence of f_ϵ and (iv) Influence of free stream viscosity ratio. Evaluation of the PANS method in terms of each of these parameters is important in its own way.

Scale-resolving methods are well-known to show sensitivity to the discretization schemes. [Constantinescu and Squires \(2003a\)](#) showed that the results of both LES and DES, despite having adequately refined grid and time steps, change considerably with change of discretization scheme. Ascertaining the extent of influence of the discretization scheme on PANS simulation of the flow past a sphere is thus important. Toward this objective, we evaluate the performance of the three advanced discretization schemes available in ANSYS FLUENT: MUSCL, second order upwind (SOU) and bounded central difference (BCD) scheme. In Section 5b, we present a comparative study of the results from simulations X03, X04 and X05 to evaluate the influence of the discretization scheme on PANS results. While simulation X03 uses MUSCL scheme; X04 and X05 employ SOU and BCD scheme respectively. Except for the discretization scheme, other parameters of these three simulations are identical.

Turbulent features of incoming freestream flows are often not completely characterized in many engineering flow scenarios. CFD simulations of such flow fields are often done with a user-assumed turbulent viscosity ratio. This could prove to be a major source of uncertainty in the final CFD results, if the turbulence model/computational methodology has significant sensitivity to the inlet viscosity ratio. This problem has been observed especially in unsteady RANS simulations of massively separated flows ([Han *et al.* 2012](#)). Thus, in order to minimize the overall uncertainty of CFD simulations, it is desirable to have a certain level of robustness in computational methodology and an ensuing low sensitivity to the chosen inlet viscosity ratio and indeed PANS is also an unsteady simulation paradigm, its closure models are extracted from existing RANS models. Thus, it is quite appropriate that PANS methodology is also carefully evaluated in terms of sensitivity to the freestream turbulent viscosity ratio. Flow past a sphere, with its inherently unsteady and massively separated flow field, makes an excellent test bed for such a numerical experiment. With this motivation, in Section 5c

we compare the results from simulations X03, X06 and X07. These simulations are identical except for the initial chosen value of the turbulent to laminar viscosity ratio (Eq. 11). To the best of authors' knowledge, no such sensitivity study for PANS has been performed in context of any flow field so far.

The PANS method is supposed to have the ability of releasing more scales of motion as the value of f_k is reduced. We test whether this expected behaviour is indeed demonstrated by PANS while simulating a complex field flow such as that past a sphere. In Section 5d, we perform a systematic study to evaluate the influence of f_k on PANS simulation of flow past a sphere. For this study, results from simulations X03, X08 and X09 have been compared. These simulations differ only in terms of the value of filter parameter f_k .

At high enough Reynolds number, wherein the turbulence kinetic energy spectrum is broad-based with a well-defined inertial range, dissipation rate can be expected to be predominately concentrated at the smallest scale of motion. For such a flow field, it is reasonable to set $f_\epsilon = 1$ in a PANS simulation. However, if the Reynolds number is not high enough, significant dissipation may occur in inertial range as well. This would necessitate a sub-unity value of f_ϵ ([Girimaji and Abdol-Hamid 2005](#)). Since at the onset we don't know if the value of $Re = 1.14 \times 10^6$ is high enough to set $f_\epsilon = 1$, in Section 5e we examine the influence of second filter parameter f_ϵ on our PANS simulation. We perform this examination at two different values of f_k . Simulations X03 and X10 examine the influence of f_ϵ with f_k fixed at 0.5, where as simulations X08 and X11 examine the influence of f_ϵ with f_k fixed at 0.7.

4.1 Quantities of Interest

In this paper, extensive evaluation of the results is performed in terms of: (i) time-averaged value of drag coefficient, (ii) mean pressure coefficient distribution, (iii) mean skin friction coefficient distribution, (iv) contours of viscosity ratio and (v) visualization of dominant flow structures in instantaneous flow fields. Each simulation is performed over an extended duration of time to ensure that the influence of initial condition on the flow field is removed and reliable flow statistics can be extracted by performing time-averaging. Each simulation is run for 60 D/V_∞ time units. Results of the first 30 D/V_∞ time units are discarded. Subsequently, time averaging is performed using the results of next 30 D/V_∞ time units.

The mean flow fields is evaluated in terms of parameters like mean drag coefficient, mean coefficient of pressure and mean skin friction coefficient:

$$C_D = \frac{\langle \bar{F}_x \rangle}{0.5\rho V_\infty^2 A}; C_p = \frac{\langle \bar{p} \rangle - p_\infty}{0.5\rho V_\infty^2}; C_f = \frac{\langle \bar{\tau}_w \rangle}{0.5\rho V_\infty^2}.$$

where the overhead represents the time-averaged value of a quantity and A represents reference area ($= \pi D^2/4$). The symbol P_∞ represents freestream pressure.

The instantaneous flow field is studied using viscosity ratio contours and iso-surfaces of vorticity. The iso-surfaces are generated using so-called Q-criterion (Hunt *et al.* 1988), where:

$$Q = \frac{|\Omega_{ij}\Omega_{ij}| - |S_{mn}S_{mn}|}{2}; \Omega_{ij} \text{ is filtered rotation-rate tensor and } S_{mn} \text{ is filtered strain-rate tensor:}$$

$$\Omega_{ij} = \frac{1}{2} \left(\frac{\partial U_i}{\partial x_j} - \frac{\partial U_j}{\partial x_i} \right); S_{mn} = \frac{1}{2} \left(\frac{\partial U_m}{\partial x_n} + \frac{\partial U_n}{\partial x_m} \right).$$

5. RESULTS AND DISCUSSION

This section is organized into five subsections. In subsection 5a we first present our time-step study. Subsequently, in subsections 5b, 5c, 5d and 5e we present our studies on the influence of discretization schemes, influence of freestream viscosity ratio, influence of filter parameter f_k and influence of filter parameter f_ϵ , respectively.

5.1 Time-Step Convergence

Simulations X01, X02 and X03 are employed for time-convergence study. Corresponding CFL number of these simulations are 4, 2 and 1 respectively (based on the smallest grid dimension).

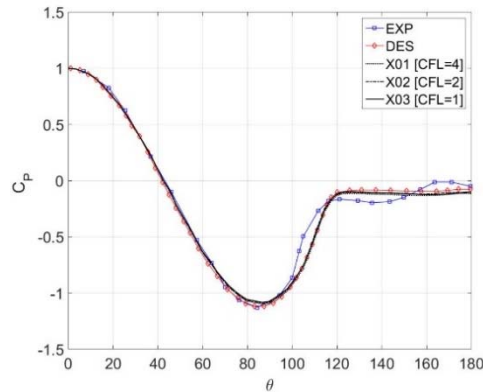


Fig. 3. Cp distribution [X01, X02 and X03]

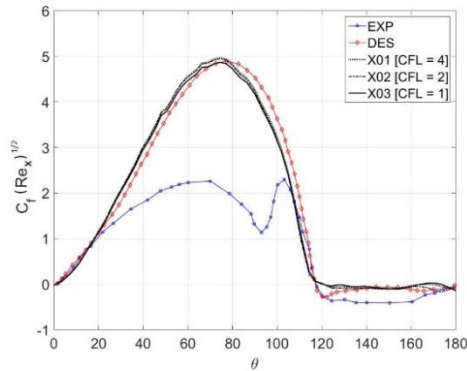


Fig. 4. Cf distribution [X01, X02 and X03]

In Fig. 3, we show the mean pressure distribution, and in Fig. 4, we show the mean skin friction coefficient distribution obtained from simulations X01, X02 and X03. Further, results from experiments (Achenbach 1974) and DES results (Constantinescu and Squires 2004) are also presented. Over the range $0^\circ < \theta < 80^\circ$, there is no discernible difference between the results from these simulations – neither in mean C_p nor in mean C_f . In the range $100^\circ < \theta < 180^\circ$, some differences between the results of these simulations are observed, especially in the separated region ($120^\circ < \theta < 180^\circ$). However, the differences are not very significant. In fact, the difference between simulations X02 [CFL=2] and X03 [CFL=1] is smaller than that between X01 [CFL=4] and X02 [CFL=2].

In Table 5a, we present the value of overall drag coefficient. The experimentally measured value of C_D at the chosen Reynolds number is 0.120. The difference in value of C_D between simulation X01 and simulation X03 is 2.5% of experimental value, whereas the difference in C_D values between simulation X02 and X03 is 0.83% of experimental value. Clearly, reduction in time-step reduces the error. Thus, it can be concluded that results have ceased to differ significantly with reduction in the time-step.

Table 5a CFL Study

Case	f_k	f_ϵ	CFL	C_D
X01	0.5	1	4	0.141
X02	0.5	1	2	0.139
X03	0.5	1	1	0.138
Experimental (Achenbach 1974)				0.120
DES (Constantinescu and Squires 2004)				0.104

Based on these observations we deem the non-dimensionalized time-step of 0.0009 (CFL = 1) to be adequate for performing a PANS simulation with $f_k = 0.5$ on our grid. All other simulations in the paper employ the same time-step. To present our results in perspective, we have included experimental results (Achenbach 1974) and DES results (Constantinescu and Squires 2004) as well. Clearly, PANS results show gross disagreement with experimental case especially in terms of C_f distribution. Indeed, our results show behaviour similar to what is observed in DES (Constantinescu and Squires 2004). Accurately capturing of variation of C_f is a challenge for scale-resolving methods in general. The goal behind the comparisons presented in this subsection (Figs. 3, 4 and Table 5a) is to confirm the adequacy of time-step convergence only. Agreement/disagreement with experimental

and DES data is the subject of discussion for later subsections.

5.2 Influence of Discretization Schemes

To examine the influence of discretization schemes, we present results from simulations X03, X04 and X05. The third-order MUSCL, second order Upwind and second-order BCD schemes have been employed in simulations X03, X04 and X05 respectively. In each of these simulations, the filter-control parameters f_k and f_ϵ have been chosen as 0.5 and 1 respectively.

In Table 5b, we present the time-averaged value of overall drag coefficient from these simulations. Among the three discretization schemes, performance of BCD scheme shows the largest deviation from experimental results with its C_D value = 0.187, which is 55.83% overestimated relative to the experimental value of 0.120. With SOU scheme the performance significantly improves, however the best performance is observed in simulation X03 which employs MUSCL scheme. The C_D value computed using MUSCL scheme is 0.138 which is 15% different from that of experimental observation. Clearly, the performance of MUSCL scheme is much superior ($C_D = 0.138$ vs. the experimental value of $C_D = 0.120$) to BCD ($C_D = 0.187$) and marginally better than SOU ($C_D = 0.141$) scheme.

Table 5b Discretization Scheme Study

Case	f_k	f_ϵ	Scheme	C_D
X03	0.5	1	MUSCL	0.138
X04	0.5	1	SOU	0.141
X05	0.5	1	BCD	0.187
LES (Kim and Choi 2001)				0.139
EXP (Achenbach 1974)				0.120
DES (Constantinescu and Squires 2004)				0.104

In the Table 5b, we have presented results from LES simulation (Kim and Choi 2001) and DES (Constantinescu and Squires 2004) as well. The LES results (Kim and Choi 2001), like PANS simulation, overestimate the C_D value. DES results, on the other hand underestimate mean C_D . The absolute percentage of error of DES and LES results when compared to the experimental observations are 13% and 15% respectively. Clearly, PANS (simulation X03) performance is quite comparable to that of the LES and DES results.

In Fig. 5, we present the variation of C_p along the mid-plane of the sphere as a function of θ . Over the region of $0^\circ < \theta < 60^\circ$, results from

simulations X03, X04 and X05 are indistinguishable, and these in turn are in excellent agreement with both DES as well as the experimental results. Over the region of $60^\circ < \theta < 100^\circ$, MUSCL results show better agreement with experimental and DES data compared to SOU and BCD scheme. Over the region of $100^\circ < \theta < 180^\circ$, all three schemes show departure from the experimental data. However, over this region MUSCL scheme still performs better than SOU and BCD, because the former shows good agreement with at least the DES results.

In Fig. 6, we present mean skin friction coefficient distribution. All numerical results (PANS as well as DES) show gross disagreement with experimental data of Achenbach (1974) (except over $0^\circ < \theta < 20^\circ$ & $100^\circ < \theta < 120^\circ$). Prediction of C_f is closely linked to the wall treatment strategy adopted in a CFD solver. Accurate prediction of skin friction coefficient in flows with massive three-dimensional separation has not been conclusively addressed yet by the CFD community at large -whether in the paradigm of RANS or in the paradigm of scale resolving methods like LES, DES (Constantinescu and Squires 2003a). PANS, being a relatively newer method, thus, also suffers from such a shortcoming- as revealed in our simulations. We have used the two-layer k-epsilon strategy (Chen and Patel 1988) for our calculations, and our results show that this approach is inadequate in capturing the skin friction coefficient in three-dimensionally separated flow field past a sphere. A better wall treatment strategy-specifically designed for three dimensional separated regions is certainly required to improve prediction of C_f in a flow such as that past a sphere. Nonetheless, among the three PANS simulations, clearly MUSCL scheme seems to agree with the DES results closer than SOU and BCD scheme. Among the three schemes, performance of the BCD scheme is the worst, especially in the aft region where separated flow exists.

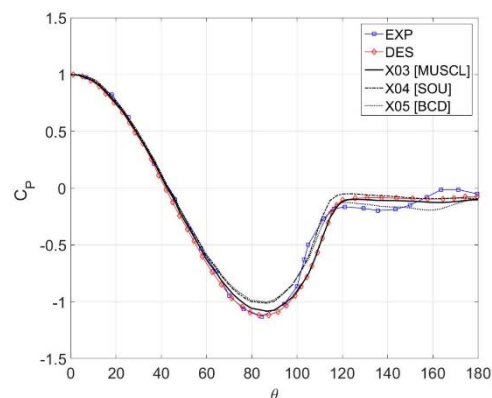


Fig. 5. C_p distribution [X03, X04 and X05]

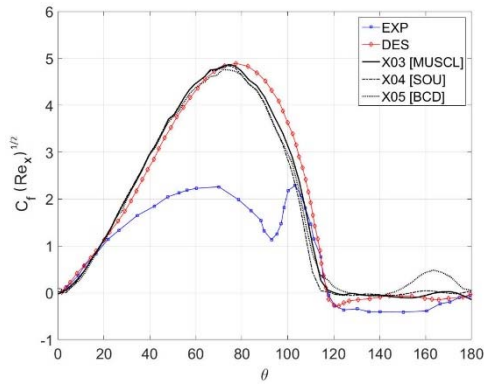


Fig. 6. C_f distribution [X03, X04 and X05]

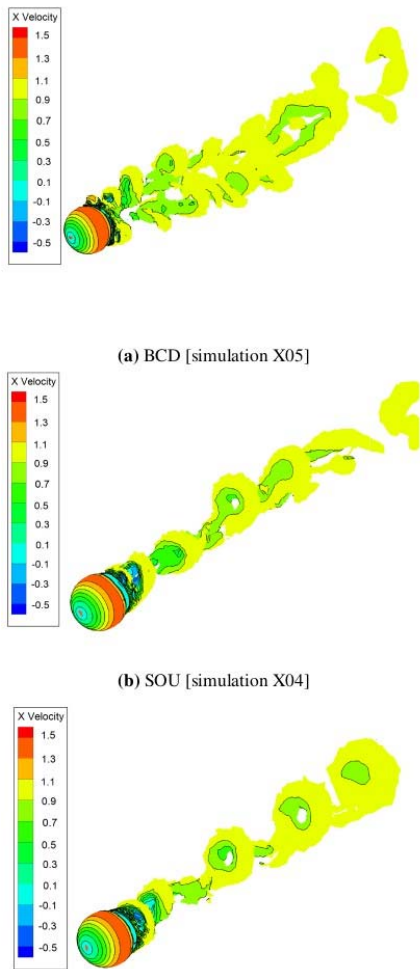


Fig. 7. Instantaneous vortical structures

Further evaluation of the schemes, is performed in terms of the vortical structures around the sphere. In Figs. 7a, 7b and 7c we present the iso-surfaces of Q colored with contours of instantaneous axial velocity. At the Reynolds number of 1.14×10^6 , Constantinescu and Squires (2004) report identification of horseshoe vortices. A comparison of the results from our three simulations clearly shows that the MUSCL scheme is the most successful in capturing well-defined horseshoe vortices in the wake. While simulation X04 (SOU) shows more diffused

vortical structures in comparison to MUSCL scheme (simulation X03); BCD scheme (simulation X05) shows two vortex streets, which is grossly inconsistent with results observed in DES or in experiments [Constantinescu and Squires (2004), Achenbach (1974)].

In Figs. 8a, 8b and 8c we present the contours of viscosity ratio $[v_u/v]$. Note that, like Constantinescu and Squires (2004), each of these figures is shown in the plane of the resultant lateral force. All three figures have been plotted using the instantaneous flow field at the same chosen time instant ($t = 60 D/V_\infty$) and the contour levels are generated automatically based on the range of data available in the flow field around the sphere region.

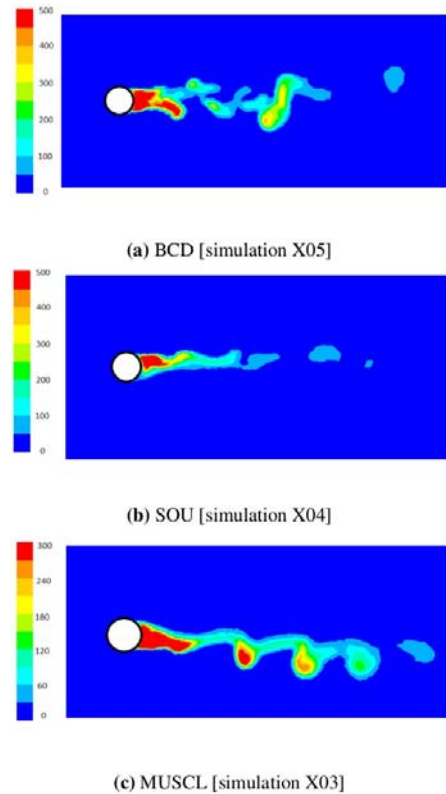


Fig. 8. Viscosity ratio contours

Among the three schemes, again the MUSCL scheme seems to be producing results which are in better agreement with DES results (Constantinescu and Squires 2004) rather than SOU or BCD scheme. At the Reynolds number of 1.14×10^6 , Constantinescu and Squires (2004) present that the wake structure show a prominent asymmetry: the wake is misaligned with the flow direction. Clearly, MUSCL scheme captures this effect more predominantly than either BCD or SOU. The contour maps displayed in Figs. 8a, 8b and 8c also indicate that the viscosity ratio is, in general, lower with MUSCL scheme as compared to simulation with BCD or SOU scheme. In a scale-resolving method, it is indeed desirable to have a lower viscosity ratio in the wake region to

successfully release more scales and features of fluid motion. Our results demonstrate that the MUSCL scheme is achieving this goal better than the other two schemes.

Summarizing this subsection, we conclude that the performance of the third-order MUSCL scheme is superior to both the BCD scheme and the SOU scheme in simulating flow past a sphere using PANS methodology. Among these three discretization schemes, performance of the second order BCD scheme is found to be the most dissipative and the least accurate. Based on these findings, all the remaining PANS studies have been performed employing the third-order MUSCL scheme.

5.3 Influence of Freestream Viscosity ratio

In this subsection we examine the sensitivity of PANS results on the freestream viscosity ratio. This examination is performed by comparing the results from simulations X03, X06 and X07. These simulations differ only in terms of the freestream viscosity ratio (η_r). Simulation X03 has the viscosity ratio as 10, whereas simulations X06 and X07 have the ratio as 1 and 100 respectively. The f_k value in all these simulations is 0.5 and the value of f_ϵ has been set to unity. The chosen discretization scheme is the third-order MUSCL. We study the influence of η_r on both the mean quantities and the instantaneous flow features.

Table 5c Effect of η_r Study

Case	f_k	f_ϵ	η_r	C_D
X06	0.5	1	1	0.140
X03	0.5	1	10	0.138
X07	0.5	1	100	0.141
Experimental (Achenbach 1974)				0.120
DES (Constantinescu and Squires 2004)				0.104

In Table 5c, we present mean value of C_D calculated from the results of simulations X03, X06 and X07. With $\eta_r = 1$, we get mean C_D as 0.140, whereas with $\eta_r = 100$ we get mean value of C_D as 0.141. Simulation X03, where we use $\eta_r = 10$, shows $C_D = 0.138$. Clearly, the influence of η_r is not very significant on the mean C_D value.

Fig. 9 distribution of C_p in simulations with $\eta_r = 1$ and $\eta_r = 10$ are indistinguishable, whereas the mean C_p variation of $\eta_r = 100$ simulation shows some deterioration in performance especially in the range of $60^\circ < \theta < 120^\circ$. In Fig. 10, where mean C_f is plotted, the results from simulation with $\eta_r = 10$ and $\eta_r = 100$ are indistinguishable. However, the simulation with $\eta_r = 1$ shows some deterioration of performance in the separated

region $90^\circ < \theta < 180^\circ$.

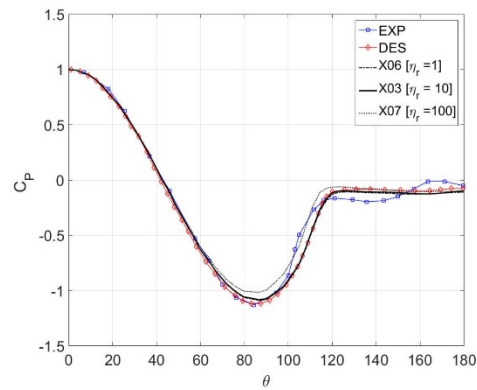


Fig. 9. C_p distribution [X03, X06 and X07]

Comparisons of mean pressure coefficient and skin friction coefficient are presented in Figs. 9 and 10. In

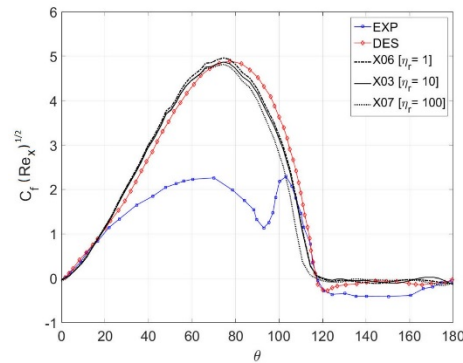


Fig. 10. C_f distribution [X03, X06 and X07]

In Figs. 11a, 11b and 11c, we present iso-surfaces of Q from instantaneous flow fields. The figures show very similar results for simulations X03 and X06 (with η_r as 1 and 10 respectively). However, the iso-surfaces obtained from simulation X06 ($\nu_u/\nu = 1$) show less sharp vortical structures especially in the near-wake region. The high value of this viscosity ratio adds dissipation to the flow field, thus leading to suppression of turbulent structures.

We conclude that the PANS paradigm, in conjugation with the two-layer $k-\epsilon$ model, shows reasonable stability of mean quantity (C_D , C_p , C_f) in response to the level of viscosity ratio in the free stream conditions. However, the instantaneous results show some mild deterioration in performance (as compared to the experimental results) at very high value of the viscosity ratio ($\eta_r = 100$). This is an important demonstration highlighting the robustness of the PANS paradigm in conjunction with the two-layer $k-\epsilon$ model in a highly complex, three-dimensional, separated flow field. Indeed Han *et al.* (2012) in their study of RANS models, find standard $k-\epsilon$ to demonstrate undesirable sensitivity to freestream viscosity ratio. However, our PANS results seem to suggest that despite the parents model being $k-\epsilon$, its PANS version shows acceptable immunity to freestream

turbulence. Overall, we judge $\eta_r = 10$ to be an optimum choice for initialization of the flow field at Reynolds number under consideration and the remaining studies of this paper performed keeping $\eta_r = 10$.

5.4 Influence of Filter Parameter f_k

PANS has been purposed as a seamless method with the inherent potential to release increasingly more scales as f_k is reduced. Such a trend has indeed been demonstrated in several flow fields [Lakshmiathy and Girimaji (2006),

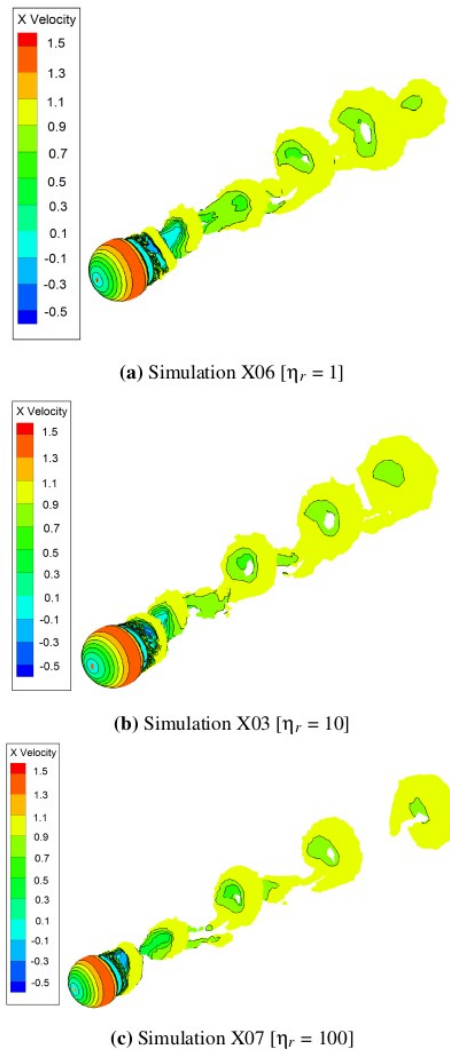


Fig. 11. Instantaneous vortical structures

Lakshmiathy and Girimaji (2010a)]. However, in this subsection we examine if PANS simulations are indeed successful in doing so in a complex, massively separated flow field such as that around a sphere as well. Towards this goal we employ three simulations (X03, X08 and X09) which differ only in terms of the chosen values of f_k . Simulation X09 employs $f_k = 1$. Since the value of other filter parameter f_ϵ is already 1, effectively, simulation X09 is an

URANS simulation. On the other hand, simulation X08 and X03 are PANS simulations with $f_k = 0.7$ and $f_k = 0.5$, respectively. The justification of this choice is discussed in detail in Section 5e.

In Table 5d we present mean C_D values from the three simulations. The experimental mean C_D value reported by Achenbach (1974) is 0.120. As the f_k value is reduced from 1 to 0.5, the mean C_D value monotonically reduces and moves closer to the experimental results of Achenbach (1974). In the table we have also presented the LES results of Kim and Choi (2001) [$C_D = 0.139$], Jindal, Long, Plassmann, and Sezer-Uzol (2004) [0.141] and DES results of Constantinescu and Squires (2004) [0.102]. Our PANS results, like the LES simulations of Kim and Choi (2001) and Jindal *et al.* (2004), overestimate the value of C_D . The DES simulation of Constantinescu and Squires (2004), on the other hand, underestimates the value of C_D . Examining the percentage difference of the C_D values (with the experimental value as the datum) we find that our simulation with $f_k = 0.5$ has error of around 15% which is equal to that of DES result (Constantinescu and Squires 2004). The LES results of Kim and Choi (2001) and that of Jindal *et al.* (2004) show error of 15.8 % and 19.1 % respectively. Clearly, the PANS simulation with $f_k = 0.5$ shows improved prediction of mean drag coefficient over the reported LES results.

Table 5d Variation of f_k Study

Case	f_ϵ	f_k	C_D
X03	1.0	0.5	0.138
X08	1.0	0.7	0.152
X09	1.0	1.0	0.190
LES (Kim and Choi 2001)			0.139
LES (Jindal <i>et al.</i> 2004)			0.143
Experimental (Achenbach 1974)			0.120
DES (Constantinescu and Squires 2004)			0.104

In Fig. 12, we present the mean C_p distribution from various simulations and experiments. Like mean C_D , mean C_p also shows maximum departure from the experimental observations in the case of URANS simulations. However, as the value of f_k is reduced, we observe an improvement in the results. Indeed, PANS result with $f_k = 0.5$ is almost indistinguishable from DES results of Constantinescu and Squires (2004). In the range $\theta < 100^\circ$, PANS with $f_k = 0.5$ shows excellent agreement with the experimental data (Achenbach 1974) as well. In the range $100^\circ < \theta < 180^\circ$, like DES (Constantinescu and Squires 2004), $f_k = 0.5$

PANS results show some departure from experimental data.

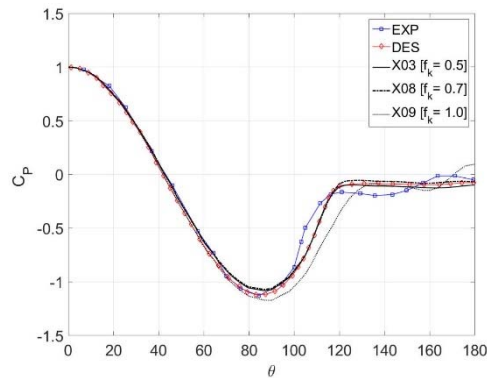


Fig. 12. C_p distribution [X03, X08 and X09]

In Fig. 13, we present the surface distribution of the mean value of C_f . As expected, the URANS results are the most inaccurate, especially in the wake region ($\theta > 120^\circ$). Again, reducing the value of f_k improves the performance of PANS results. In the region with $80^\circ < \theta < 120^\circ$, even

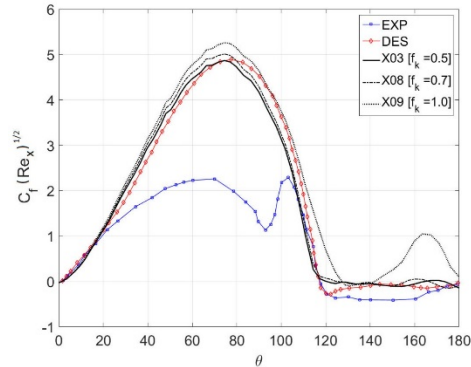


Fig. 13. C_f distribution [X03, X08 and X09]

though all numerical simulations show gross departure from the experimental observations, $f_k = 0.5$ results do show some improvement over even the DES results. At other locations, PANS result with $f_k = 0.5$ are very similar to those in DES simulation.

Further examination of the influence of f_k is performed in terms of the instantaneous flow field and turbulence structures. In Figs. 14a, 14b and 14c we present contours of viscosity ratio in the plane of the net instantaneous lateral force. As the value of f_k is reduced in the PANS paradigm, it is expected that the levels of viscosity ratio in the flow field would monotonically decrease – thus allowing smaller scales of motion to be released (resolved) in the flow field.

In Figs. 14a, 14b and 14c contours are plotted with same range of color map. Clearly, the levels of viscosity ratio are the highest in URANS simulation with $f_k = 1$. Scale levels monotonically decrease as we go to simulation X08 ($f_k = 0.7$) and then to simulation X03 ($f_k = 0.5$). This is again along the expected lines.

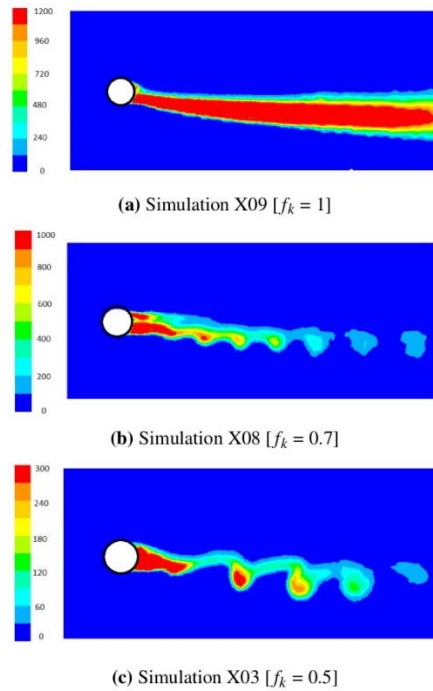


Fig. 14. Viscosity ratio contours

Further evidence of the release of more scales of motion in simulations X03 and X08, as compared to URANS simulation, can be observed in Figs. 15a, 15b and 15c, wherein we show iso-surfaces of Q-criterion from three simulations.

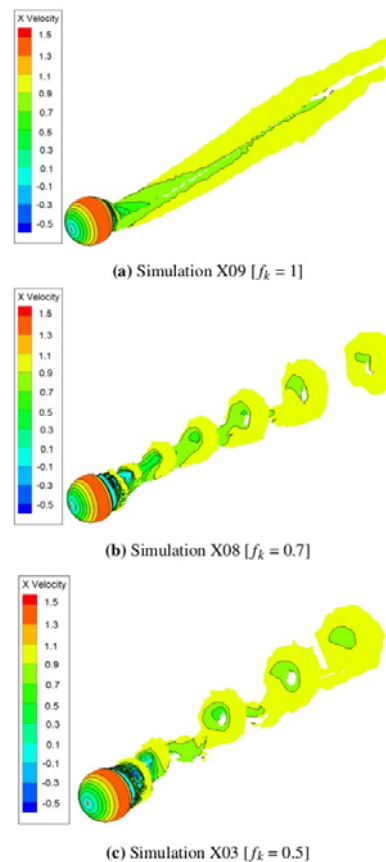


Fig. 15. Instantaneous vortical structures

With $f_k = 0.5$, simulation X03 clearly shows several horseshoe vortices being shed in the wake of the cylinder. This behaviour is in line with the results of DES (Constantinescu and Squires 2004) as well as experimental observations. Infact based on the comparison of our results and the results of Constantinescu and Squires (2004), it seems that the PANS Simulation X03 is resolving the horseshoe vortices perhaps better than even those in the DES simulations (compare our Fig. 14c with Fig. 9d of (Constantinescu and Squires 2004)). In simulation X08 with $f_k = 0.7$, the size of the horseshoe vortices decreases and they look underdeveloped. However, their presence is still very much evident. In contrast, the vortex structure captured by the URANS (simulation X09) is quite different. We do not observe any evidence of horse-shoe vortices. Instead, two counter-clockwise extended vortex tubes are seen. This is in gross disagreement with the behaviour expected at supercritical Reynolds number of 1.14×10^6 . Thus, based on our observations, we conclude that decreasing the value of f_k for flow past a sphere, PANS indeed shows a clear capability to capture the complex vortex shedding patterns expected at high Reynolds number. Further, at $f_k = 0.5$, the vortex structure seem to be better resolved than even DES results of Constantinescu and Squires (2004).

5.5 Influence of filter parameter f_ϵ

We study the influence of f_ϵ by comparing the results from simulations X03, X08, X10 and X11. Simulations X03 ($f_k = 0.5, f_\epsilon = 1$), and X08 ($f_k = 0.7, f_\epsilon = 1$) have been earlier employed in Section 5d to study the influence of f_k . These simulations use $f_\epsilon = 1$. To evaluate the influence of f_ϵ , we compare results of simulation X03 and X10, which have identical f_k ($= 0.5$) but different f_ϵ (1 and 0.5). Since all other parameters of the two simulations are identical, differences observed in these two flow fields can be attributed to the difference in the value of f_ϵ . To further understand the trend, if any, we further compare results from simulation X08 ($f_k = 0.7, f_\epsilon = 1$) and X11 ($f_k = 0.7, f_\epsilon = 0.7$).

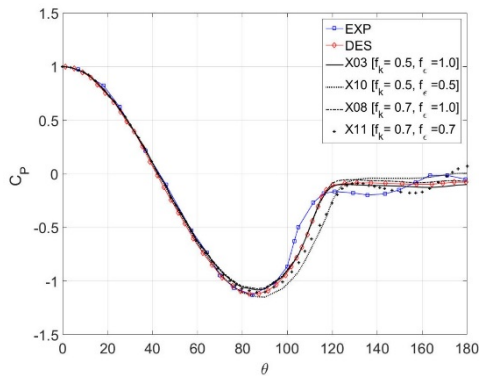


Fig. 16. C_p distribution [X03, X08, X10 and X11]

In Fig. 16, we present the distribution of mean C_p obtained from simulations X03, X08, X10 and X11. Results from simulation X03 show significant differences as compared to that from X10. Similarly, simulation X08 and X11 show differences. In the aft region of the sphere, the pressure coefficient predicted by simulations X10 and X11 (with a lower value of f_ϵ) shows significantly more error when compared to the experimental data or the DES results.

In Fig. 17, we show the variation in the mean skin friction coefficient value. Similar deterioration in performance is observed when f_ϵ is reduced. The performance of simulation X11 with $f_k = 0.7$ and $f_\epsilon = 0.7$ is much inferior to the performance shown by simulation X08 with $f_k = 0.7$ and $f_\epsilon = 1$. Similarly, some deterioration in performance is seen at $f_k = 0.5$ when f_ϵ is changed from 1 to 0.5.

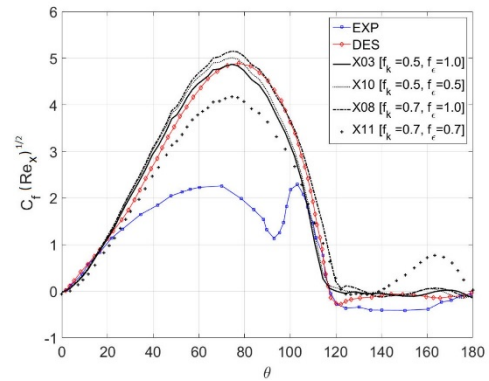


Fig. 17. C_f distribution [X03, X08, X10 and X11]

Further confirmation of the inferior performance of PANS simulations at lower values of f_ϵ is demonstrated in Figs. 18a, 18b, 18c and 18d wherein we show the vortical structure of the wake past the sphere in simulations X03, X10, X08 and X11 respectively. Clearly, lowering the value of f_ϵ while keeping the f_k value fixed, causes a deterioration in ability to capture the vortical structure. At a lower f_ϵ value, no horseshoe vortex is seen. Indeed, the vortical structure seen at a lower f_ϵ is reminiscent of the vortical structures that are observed in experiments at lower Reynolds number [Taneda (1978), Jones and Clarke (2008)].

The ability of a scale-resolving method using eddy-viscosity hypothesis relies on the influence of filter-controlling parameters to appropriately lower the value of eddy viscosity. In PANS, this control is achieved by choosing appropriate values of f_k and f_ϵ . A lower value of f_k is expected to reduce the level of turbulence kinetic energy in the flow field by primarily subduing the production mechanism. Lowering the value of f_ϵ , on the other hand, reduces dissipation, which in turn increase accumulation of unresolved kinetic energy. Thus, lowering the value of both f_k and

f_ϵ has counteracting effects on the unresolved kinetic energy and in turn, on the eddy viscosity.

At very high Reynolds number, it is indeed prudent to choose the maximum possible value of f_ϵ ($=1$) because it is reasonable to expect that the filter cut-off lies far right to the dissipation scales of the turbulence kinetic energy spectrum. However, if the Reynolds number is not ‘adequately high’, the separation between the cut-off scale of turbulence kinetic energy and dissipation scales may not be large. In such a case, setting $f_\epsilon = 1$ may not be the correct choice, and choosing a subunity value of f_ϵ may

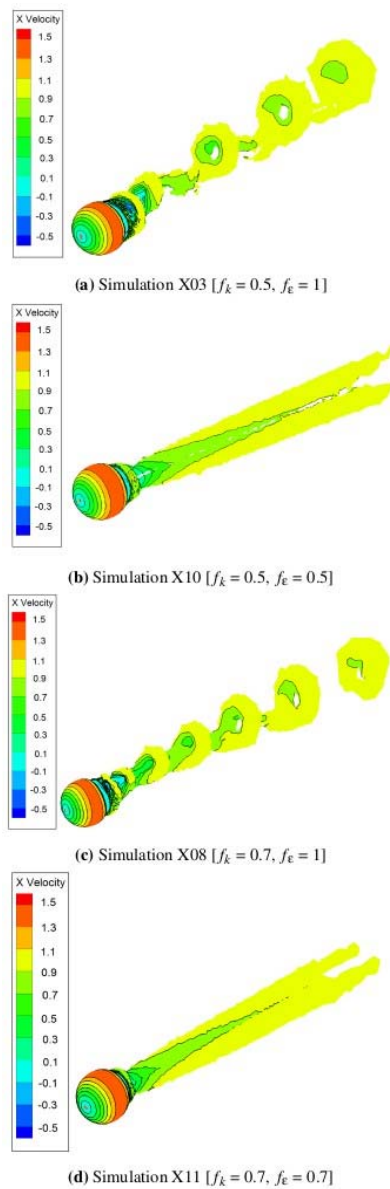


Fig. 18. Instantaneous vortical structures

lead to superior performance of the PANS methodology. On the other hand, at a high Reynolds number, if f_ϵ is chosen to be too low, then there is a risk of reducing the dissipation values so much that it unrealistically counter-

balances the reduction in production achieved by a lower value of f_k . In extreme cases, the dissipation rate may be reduced so much that large values of turbulence kinetic energy accumulate in the flow field (despite a subunity value of f_k) causing the turbulence viscosity to become comparable with the URANS levels. Such a situation will lead to suppression of scales and the simulated flow field may resemble more like a URANS simulation. Thus, it is important to choose the correct balance between f_k and f_ϵ values.

Indeed, Lakshmipathy and Girimaji (2010b) in their study of the performance of PANS method, demonstrate that while at Reynolds number = 1.4×10^5 the performance of PANS simulation is superior with $f_\epsilon = 1$, the performance is superior at Reynolds number = 3900 with $f_\epsilon = 0.7$ (at the same f_k value). Since it is not at all straightforward to conjecture the optimum value of f_ϵ at a given Reynolds number, a careful study of the influence of f_ϵ is thus required.

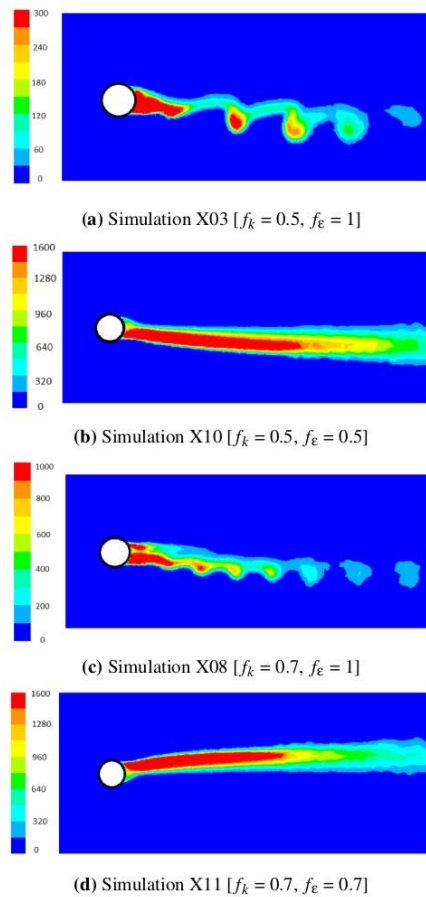


Fig. 19. Viscosity ratio contours

Results of our simulations suggest that the optimum value of f_ϵ for flow past a sphere, at Reynolds number = 1.14×10^6 , is indeed 1. When a lower value of f_ϵ is chosen, dissipation reduces – thus counteracting the reduction in production achieved by sub-unity f_k value. This is confirmed

in Figs. 19a, 19b, 19c and 19d wherein we show the scales for the contour levels of dissipation from simulations X03, X10, X08 and X11. Clearly, simulation X03 shows more dissipation scales as compared to simulation X10. Similarly, Figs. 19c and 19d show more dissipation scales prevailing in the flow field in simulation X08 as compared to simulation X11.

6 SUMMARY

We study the performance of partially averaged Navier-Stokes (PANS) method in simulating massively separated flow field around a sphere at supercritical Reynolds number = 1.14×10^6 . Despite its geometric simplicity, flow past a sphere is acknowledged to be quite complicated due to the coexistence of numerous complex phenomena. This complexity makes this flow an excellent test bed for turbulence models and numerical schemes alike. In this work, we evaluate PANS specifically in terms of four aspects: (i) influence of filter parameter f_k , (ii) influence of filter parameter f_ϵ , (iii) influence of discretization scheme and (iv) influence of freestream turbulence viscosity ratio.

As purported, a monotonic reduction in the value of f_k systematically releases more scales of motion and takes the results closer to experiments/DES simulation. Indeed, mean quantities calculated using PANS simulations with $f_k = 0.5$ are found to be fairly close to the DES results of Constantinescu and Squires (2004).

Further, our study reveals that, like other scale resolving methods [DES (Constantinescu and Squires 2004), LES (Kim and Choi (2001), Jindal *et al.* (2004))], PANS shows significant sensitivity to the numerical schemes. The third-order MUSCL scheme is found to be superior to the SOU and BCD method – especially, in terms of resolving the horseshoe vortex system, which has been observed in experiments as well the state-of-the-art DES simulations.

Further, we find that the influence of freestream viscosity ratio does not affect the mean quantities much. However, it does influence the instantaneous flow features. Freestream viscosity ratio is indeed known to influence the preference of RANS models like $k-\epsilon$. Our investigations reveal that in comparison to the parent RANS model (in our case the standard $k-\epsilon$ model), the PANS paradigm tends to mitigate the sensitivity towards freestream viscosity ratio in the flow field.

Our study on the influence of f_ϵ on the results of PANS simulation ascertains that the Reynolds number of 1.14×10^6 is high enough to choose the value of the second filter parameter to be unity.

We demonstrate that at several f_k values, PANS performance is optimal with $f_\epsilon = 1$. At lower values of f_ϵ , kinetic energy dissipation reduces – thus annulling the advantage of reduced production achieved by lowering values of f_k .

Based on our findings, we conclude that the performance of PANS in simulating flow past a sphere is quite satisfactory. However, since some flow quantities, especially skin friction coefficient, is not captured adequately. Further improvements in PANS modelling, especially in terms of wall treatment, are required for reliably simulating three dimensional separated flows.

ACKNOWLEDGMENTS

We thank the IIT Delhi HPC facility for computational resources.

REFERENCES

- Achenbach, E. (1972). Experiments on the flow past spheres at very high Reynolds numbers. *Journal of Fluid Mechanics* 54(3), 565–575.
- Achenbach, E. (1974). Vortex shedding from spheres. *Journal of Fluid Mechanics* 62(2), 209–221.
- Aliabadi, S. and T. Tezduyar (1995). Parallel fluid dynamics computations in aerospace applications. *International Journal of Numerical Methods in Fluids* 21(1), 783–805.
- Bazilevs, Y., J. Yan, M. de Stadler, and S. Sarkar (2014). Computation of the flow over a sphere at $re = 3700$: A comparison of uniform and turbulent inflow conditions. *Journal of Applied Mechanics* 81(12), 121003–1–17.
- Chen, H. and V. Patel (1988). Near-wall turbulence models for complex flows including separation. *American Institute of Aeronautics and Astronautics (AIAA)* 26(6), 641–648.
- Constantinescu, G. and K. Squires (2000). Les and des investigations of turbulent flow over a sphere. *American Institute of Aeronautics and Astronautics (AIAA)* 0540(1), 1–11.
- Constantinescu, G. and K. Squires (2003a). Les and des investigations of turbulent flow over a sphere at $re = 10,000$. *Flow, Turbulence and Combustion* 70(1), 267–298.
- Constantinescu, G. and K. Squires (2003b). Turbulence modeling applied to flow over a sphere. *American Institute of Aeronautics and Astronautics (AIAA)* 41(9), 1733–1742.
- Constantinescu, G. and K. Squires (2004). Numerical investigations of flow over a sphere in the sub-critical and supercritical

- regimes. *Physics of fluids* 16(5), 1449–1466.
- Drikakis, D. (1995). *Development and implementation of parallel high resolution schemes in 3d flows over bluff bodies*.
- Gebing, H. (1992). *Numerische simulation und topologisch-physikalische analyse der instationären, dreidimensionalen, abgelösten wirbelströmungen an einer kugel und an rotationsellipsoiden*. Ph.D. Thesis, Georg-August-Universität, Göttingen, Germany.
- Germano, M. (1992). Turbulence: the filtering approach. *Journal of Fluid Mechanics* 238, 325–336.
- Girimaji, S. S. (2006). Partially-averaged navier-stokes model for turbulence: A reynolds-averaged navier-stokes to direct numerical simulation bridging method. *Journal of Applied Mechanics* 73(3), 413–421.
- Girimaji, S. S. and K. S. Abdol-Hamid (2005). Partially averaged navier–stokes model for turbulence: implementation and validation. *AIAA paper* 502, 2005.
- Han, X., P. Sagaut, and D. Lucor (2012). On sensitivity of rans simulations to uncertain turbulent in-flow conditions. *Computers & Fluids* 61, 2–5.
- Hunt, J. C., A. A. Wray, and P. Moin (1988). *Eddies, streams, and convergence zones in turbulent flows*.
- Jindal, S., L. N. Long, P. E. Plassmann, and N. SezerUzol (2004). Large eddy simulations around a sphere using unstructured grids. *AIAA Paper* 2228, 1–3.
- Johnson, T. and V. Patel (1999). Flow past a sphere up to a reynolds number of 300. *Journal of Fluid Mechanics* 378, 19–70.
- Jones, D. and D. Clarke (2008). *Simulation of flow past a sphere using the fluent code*. Technical report, Defense Science and Technology Organization Victoria (Australia) Maritime Platforms Div.
- Kalro, V. and T. Tezduyar (1998). 3d computation of unsteady flow past a sphere with a parallel finite element method. *Computer Methods in Applied Mechanics and Engineering* 151(1-2), 267–276.
- Kim, D. and H. Choi (2001). *Large eddy simulation of turbulent flow over a sphere using an immersed boundary method*. Technical report, Seoul National Univ (Korea) School of Mechanical and Aerospace Engineering.
- Kim, H. and P. Durbin (1988). Observations of the frequencies in a sphere wake and of drag increase by acoustic excitation. *The Physics of fluids* 31(11), 3260–3265.
- Lakshminpathy, S. and S. S. Girimaji (2006). Partially-averaged navier-stokes method for turbulent flows: k- ω model implementation. *AIAA paper* 119, 2006.
- Lakshminpathy, S. and S. S. Girimaji (2010a). Partially averaged navier–stokes (pans) method for turbulence simulations: flow past a circular cylinder. *Journal of Fluids Engineering* 132(12), 121202.
- Lakshminpathy, S. and S. S. Girimaji (2010b). Partially averaged navier-stokes (pans) method for turbulence simulations: flow past a circular cylinder. *Journal of Fluids Engineering* 132(12), 121202.
- Mansoorzadeh, S., C. Pain, C. De Oliveira, and A. Goddard (1998). Finite element simulations of incompressible flow past a heated/cooled sphere. *International journal for numerical methods in fluids* 28(6), 903–915.
- Schmidt, M. (2002). *Grobstruktursimulation turbulenter Strömungen auf unstrukturierten Gittern mit einer parallelen Finite-Volumen-Methode*. Arbeitsbereiche Schiffbau der Techn. Univ.
- Seidl, V., S. Muzaferija, and M. Perić (1997). Parallel dns with local grid refinement. *Applied Scientific Research* 59(4), 379–394.
- Shen, W. and T. Loc (1997). Numerical method for unsteady 3d navier-stokes equations in velocity-vorticity form. *Computers & fluids* 26(2), 193–216.
- Shirayama, S. and K. Kuwahara (1992). Flow past a sphere- topological transitions of the vorticity field. *AIAA Journal* 30(2), 349–358.
- Suman, S. and S. S. Girimaji (2010). On the invariance of compressible navier–stokes and energy equations subject to density-weighted filtering. *Flow, Turbulence And Combustion* 85(3), 383–396.
- Taneda, S. (1978). Visual observations of the flow past a sphere at reynolds numbers between 104 and 106. *Journal of Fluid Mechanics* 85(1), 187–192.
- Tomboulides, A. G., S. Orszag, and G. E. Karniadakis (1993). Direct and large eddy simulations of axisymmetric wakes. *AIAA paper* 546.
- Tomboulides, A. G. and S. A. Orszag (2000). Numerical investigation of transitional and weak turbulent flow past a sphere. *Journal of Fluid Mechanics* 416, 45–73.